J. Eur. Opt. Society-Rapid Publ. 2024, **20**, 40
© The Author(s), published by EDP Sciences, 2024
https://doi.org/10.1051/jeos/2024043 Available online at: https://jeos.edpsciences.org

Journal of the European Optical Society-Rapid Publications

RESEARCH ARTICLE

OPEN ACCESS

Additively manufactured structures for precise and robust mounting of optical elements

Patrick Pfuhl* and Markus Degünther

Optikzentrum Wetzlar, Technische Hochschule Mittelhessen – University of Applied Sciences, Wilhelm-Leuschner-Straße 13, 61169 Friedberg, Germany

Received 13 August 2024 / Accepted 15 October 2024

Abstract. The design freedom of Additive Manufacturing offers new opportunities for the design of mounting structures of optical systems, which are not feasible for conventional manufacturing approaches, thus opening up new areas of application for optical systems. We use this to develop a fully monolithic mounting structure for precise positioning of the optical elements, while simultaneously increasing their robustness against harsh environmental conditions. We additively manufacture such a mounting structure for an imaging lens and evaluate its optical performance with interferometric measurement of its wavefront, before and after applying a mechanical shock to the entire system. The results indicate a centering accuracy better than 6 µm, both in the initial positioning as well as the subsequent repositioning after a mechanical shock of 15G.

Keywords: Optomechanics, Monolithic, Additive manufacturing, Alignment.

1 Introduction

The continuous improvements in additive manufacturing (AM), particularly in terms of manufacturing accuracy and surface quality, have led to increased research efforts to utilize it for optical applications [1, 2]. For micrometer optics it is possible to print complete optical systems in only one piece using the commercially available two-photon grayscale lithography [3–5]. For larger optics, other additive manufacturing processes are required, as the layer-by-layer process requires a compromise between surface quality, manufacturing speed and accuracy [6]. To achieve a typical optical surface roughness of sub 10 nm additional post-processing steps such as polishing, coating are needed, which prevents fully monolithic optical systems [7, 8]. A promising research approach for such larger elements are continuous projection micro-stereolithography processes, which still require a finalizing meniscus coating of the their optical surfaces [9].

Nevertheless, optical systems can still benefit significantly from the potential of AM by producing their mounting structures and optomechanical components. So far, AM is commonly used in research and education, with a focus on reprints of existing optomechanical components that need to be readily available, adjustable and of low-cost [10–13]. However, the inherent design freedom of AM allows to realize components that simplify the assembly and achieve a higher system integration by incorporating new functions to improve their performance [14–16]. The general usefulness of these approaches for optomechanical systems have already been demonstrated [17–20].

We take advantage of the design freedom of AM to build robust optics that perform well even under harsh environmental conditions. Our approach is to design a fully monolithic mounting structure that supports all elements of the optical system, such as lenses, mirrors, prisms or other optical elements. Firstly, this increases the systems robustness when compared to classical multi-component optomechanics. Secondly, the alignment of the various elements essentially only depends on the accuracy and resolution of the 3D-printer. Finally, the individualization of AM allows to compensate individual element tolerances, such as inner decentration, by adapting the mounting structure accordingly.

In principle, this kind of mounting concept could be realized by using printed mechanical references, like imprinting the optical elements or using fittings as alignment surfaces [21–23]. However, the highest achievable positioning is limited by the accuracy of suitable and commercially available 3D printing processes, which is typically up to 10–40 µm for polymer material jetting printers and up to 30–100 µm for powder bed metal printers [24]. Therefore, we use the force equilibrium of deflected spring elements to position the optical element. Geometrical deviations due to the additive manufacturing process have only a small influence on the resulting spring stiffness. When combined with the symmetrical mount design, this enables positioning accuracies below the printer resolution. The springs position

* Corresponding author: patrick.pfuhl@mnd.thm.de

This is an Open Access article distributed under the terms of the Creative Commons Attribution License (https://creativecommons.org/licenses/by/4.0), which permits unrestricted use, distribution, and reproduction in any medium, provided the original work is properly cited.

and fix the optical elements until the maximum allowable acceleration during its usage is reached. Larger accelerations and mechanical shocks due to impacts, are then absorbed with elastic deformation by the springs holding the optical element. Hence, deformations only occur above the specified operating acceleration, protecting it from damage. After the shock event the forces are the same as before and the deflections of the springs return to their original position and thus any displacement is reversed.

In the following, we describe and discuss our design approach and layout in detail. For the intended proof of concept we designed such a monolithic mounting structure for an imaging lens and produced it from a polyacrylic polymer using a material jetting 3D-printer. Although the material is not ideal for the long term application in mounting structures under harsh conditions, particularly as polymers tend to plastically deform under longer applied mechanical loads due to creeping effects, the manufacturing process is optimal for our purpose. Other usable and commercially available powder bed printers with sufficiently large build volumes for processing more suitable materials, such as aluminium or steel, still have a lower accuracy and more difficult post-processing is required. However, the reason for using this 3D-printer is the transferability of the conceptual proof, obtained from investigations on polymer structures to future structures made of other materials by adapting the spring dimensions. Finally, we evaluate and compare the optical performance of the triplet lens through interferometric measurements with the simulation, both before and after subjecting the entire system to mechanical shock.

2 Fully monolithic and additively manufactured mounting structures

2.1 Mechanical mounting domains of optical elements in optical systems

Optical systems comprise the optical elements and the mounting structure. Optical elements manipulate the light according to system application and specification, usually realized with lenses, mirrors, prisms and filters. The main tasks of the mounting structure are to position the optical elements precisely and provide protection against environmental influences such as pollution, temperature fluctuations and mechanical loads. A mounting structure can be split into two mechanical design domains, the direct and indirect mounting domain, sketched in Figure 1. Direct mounting is the joining of an optical element with a mechanical structure. It provides the necessary features to determine and fix its position. Indirect mounting is the connection between multiple directly mounted elements defining their positions in respect to each other. It should be emphasized that the domain split is to be understood conceptually, but not necessarily as a split into different mechanical parts.

2.2 Basic design of fully monolithic direct mounting structures

Due to its design freedom, AM enables the design and fabrication of mounting structure concepts, which are too complex or even impossible to produce with conventional subtractive manufacturing techniques. Robust optomechanical systems can be designed by combining the direct and indirect mounting domain into one monolithic structure. To provide sufficient clearance during the insertion of optical elements, the structural features that clamp and secure them must be flexible and retractable. Thus, these clamping structures are implemented as spring elements that allow for reversible deformations.

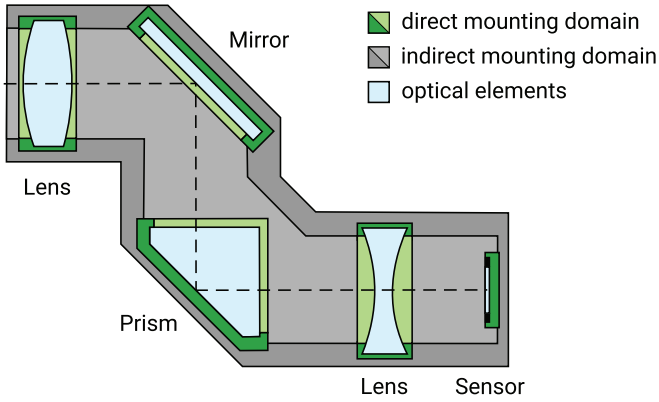

Figure 1. Principle cross-sectional sketch of a folded optical system. It comprises the optical elements (blue) and the mounting structure. The mounting structure is split into its two design domains: direct mounting (green) and indirect mounting (grey). Direct mounting is the joining of optical elements and the mounting structure, which determines and fixes their position. Indirect mounting connects those mounted elements and determines their position in relation to each other.

We demonstrate our principle approach with lenses, but it can be easily adapted to all other kinds of optical elements. The force diagram for the fully monolithic mounting concept is shown in Figure 2. The lens gets axially aligned by pushing it against a mechanical reference with the axial preload F_{preload}. Centering is ensured by balancing the radially arranged spring forces $F_{\mathrm{rad.l}}$ and $F_{\mathrm{rad.r}}$. A decentered lens causes different deflections of the clamping springs and the resulting force, which is proportional to the deflection difference, pushs the lens back into the centered position. As the lens decentration decreases, so does the imbalance in radial force. Once this imbalance becomes smaller than the resulting friction force of $R_{\mathrm{pos.l}}$ and $R_{\mathrm{pos.r}}$, the moving lens will stop and remain in this still not perfectly centered position.

To achieve a higher passive positioning accuracy we have to either reduce the friction or increase the radial forces and thus the radial spring stiffness. The magnitude of the friction force depends on the applied axial preload and the static friction coefficient between the optical element and the mounting structure. The static friction coefficient is a fixed system parameter which is difficult to modify. Thus, the axial preload has to be minimized to such an extent that the lens is just barely but reliably pressed against the mechanical stop. On the other hand, it requires radially stiff springs to accurately align the lens.

The achievable positioning accuracy is calculated according to the force diagram as a function of the axial

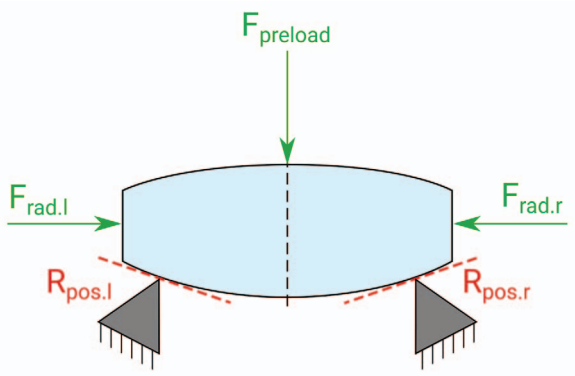

Figure 2. Force diagram to mount lenses in a fully monolithic mount with clamping springs. We sketch our approach in a plane only, but in the full three-dimensional case these structures are preferably arranged with an azimuthal distance of 120. The axial preload $\boldsymbol{F}_{\mathbf{preload}}$ presses the lens against the mechanical reference (grey), which aligns the lens axially and induces the friction forces $\boldsymbol{R}_{\mathbf{pos.l}}$ and $\boldsymbol{R}_{\mathbf{pos.r}}$, here marked as their line of action. To precisely align the lens, the friction has to be overcome by the radial force difference between $\boldsymbol{F}_{\mathbf{rad.l}}$ and $\boldsymbol{F}_{\mathbf{rad.r}}$.

preload and the radial spring stiffness, as expressed in equation (1):

$$2 \cdot \delta_{\mathrm{pa}} \cdot k_{\mathrm{radial}} = \mu_{\mathrm{s}} \cdot F_{\mathrm{preload}} \tag{1}$$

δ_{pa} represents the deflection difference of the radial springs, which remains due to the finite friction forces, and thus it is identical with the positioning accuracy. The minimum required axial preload F_{preload} is calculated by multiplying the expected maximum acceleration, resulting from shocks and vibrations during the use of optics in harsh environments, with the mass of the lens. It induces the friction forces between mounting and lens with the static friction coefficient μ_{s}. The radial force imbalance has to exceed the resulting friction force, even for small deflections δ_{pa} with its radial spring stiffness k_{radial} to accurately position the lens.

Larger accelerations, caused for example by shocks during transport or assembly, are absorbed as elastic deformation by the spring elements and protect the lenses from damage. This results in a temporary displacement of the lens, which is subsequently pushed back by the imbalance of forces. Thus, any displacement is reversed, restoring the optics to full functionality.

The achievable positioning accuracy is plotted as a function of axial preload and radial spring stiffness in Figure 3. Since small spring deflections are assumed, the spring stiffness can be considered linear. As the friction coefficient increases, a larger radial spring stiffness is necessary to obtain the same positioning accuracy at the same axial preload. This is due to the direct correlation between the friction coefficient and resulting friction, leading to a larger remaining decentration. Furthermore, reducing the axial preload also increases the positioning accuracy, as the resulting frictional force becomes lower. Holding the boundary conditions fixed while increasing the radial spring stiffness corresponds to a higher accuracy in lens positioning, because the remaining deflection difference is inversely proportional to the radial spring stiffness. This further emphasizes that the optimization target for precise lens positioning involves minimizing axial preload while maximizing radial spring stiffness. This trade-off defines our design approach to precisely position a lens and increasing its robustness against mechanical influences through the use of spring elements.

2.3 Mechanical implementation of the basic design

To precisely center a lens the radial spring stiffness has to be large to create correspondingly large force differences even for small deflection differences. Additionally, minimizing the axial preload is crucial to ensure minimal friction forces to accurately position the lens. Therefore, it is necessary to have a spring element with two distinct spring stiffnesses in axial and radial direction. In addition, to obtain the required axial preload and the resulting mechanical stresses of this spring element, it is essential to have small deflections to occur in axial and radial direction that ensure a linear deformation behaviour. Thus, it is reasonable to assume that the deflections are almost identical in both directions. The difference in resulting forces between high and low spring stiffness for the same deflection difference is depicted in Figure 4. A spring with low stiffness shows a smaller difference in resulting forces than a spring with high stiffness for the same deflection difference. One solution that satisfies these requirements is a bending spring element with a rectangular cross-section that allows to generate the axial preload independently of its radial forces. The required differences in spring stiffness result in significantly thicker springs in the radial direction than in the axial direction.

The lens is inserted into the mount along the axial direction. Once the lens is inserted, it must be held in place by sufficiently large overhangs to prevent its disassembly under large external loads. Thus, along the radial direction a significant deflection range is necessary which is not compatible with the required high radial stiffness, because the bending spring would break. Therefore, a second radial bending spring element is added. It provides the overhangs for retaining the lens in harsh environments and simultaneously allows for enough clearance to insert the lens in the mount.

The mechanical design of a fully monolithic mount is shown in Figure 5. It consists of three identical units, which are equally spaced in azimuth around the lens cylinder. Each mounting unit comprises a positioning spring element (PSE), a retaining spring element (RSE), a mechanical stop, an installation stop, a direct contacting interface and a force transmitter with hook. The spring elements have an assembly pin to move them inside the structure from outside helping to mount the lens. If necessary, the pins can be removed after assembly.

The PSE generates the radial forces as well as the axial preload to position the lens against the mechanical stop. Achieving a precise axial preload requires accurate deformation of the PSE. For this, the axial length difference between the hook and the mechanical stop in their initial position is used. The hook of the RSE and from the force

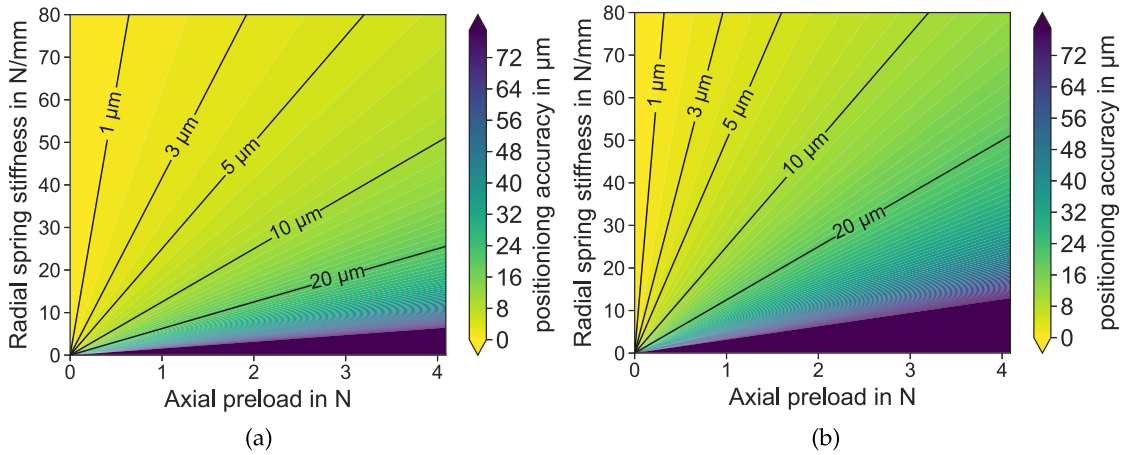

Figure 3. Plot of the positioning accuracy over axial preload and radial spring stiffness. (a) Positioning accuracy with $\mu_s = 0.25$; (b) Positioning accuracy with $\mu_s = 0.5$.

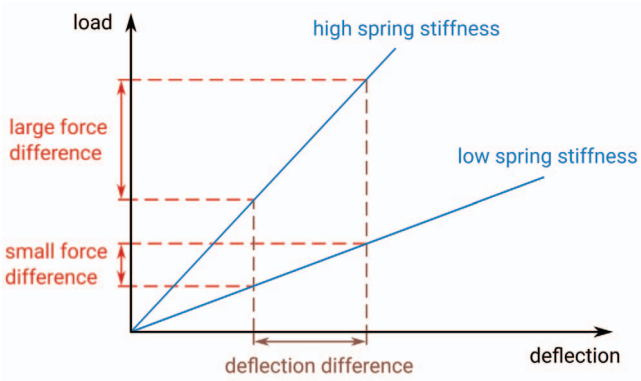

Figure 4. Principle graph of resulting force over spring deflection. With the same deflection difference, a low stiffness spring has a smaller difference in its resulting forces than a high stiffness spring.

transmitter prevent a disassembly of the lens in case a large acceleration stresses the system. It should be noted that these interfaces do not affect the positioning of the lens itself, as they are just slightly touch the optical surface and have minimal contact with it.

The assembly process comprises four steps, which are illustrated in Figure 6. For assembly, the lens is placed at first above the mount. Then the RSE is moved radially with F_{RSE} to pull the overhangs out of the diameter of the lens and open the volume for the lens insertion. Now the lens gets positioned on the installation stop, to aid with its initial position in the mount. After that, the PSEs are deflected with F_{PSE} slightly in axial as well as radial direction to be able to push the lens in between them until it touches the hook of the force transmitter. The RSEs get now positioned above the lens surface and hinder its displacement under harsh environmental strains. Due to this enforced placement, it is also possible to mount concave optical surfaces. Finally the PSE are released. The radial forces F_{rad} center the lens and the axial forces F_{preload} generated by them push it against the mechanical stop, which is designed as a sharp corner interface. The axial preload as well as the radial forces are transmitted via the direct contacting interface of the force transmitter of the PSE. It is designed as a tangent on the lens cylinder to apply the forces as line contact over its full length.

The shape of the bending springs, the magnitude of the forces and stresses are approximated with the Euler–Bernoulli beam theory. Due to its high attainable stiffness and its symmetrical design, we designed the PSE as a fixed beam. The symmetry helps to prevent buckling and twisting effects of the beam and the lens is pushed parallel to the optical axis against the mechanical stop. Since a large clearance for inserting the lens is required, the RSE is implemented as a cantilever bending spring. With other kinds of spring designs it is difficult to achieve high flexibility in one direction as well as high stiffness in the perpendicular direction in a comparatively small design volume.

Because of their large slenderness ratios and their curved design following the lens contour, the design of both spring elements is not optimal for an approximation with the Euler–Bernoulli beam theory. Thus, we performed an additional Finite Element Analysis, confirming that the movement of both spring elements can still be reasonably approximated linear. For the simulation we used the polyacrylic polymer Keyence AR-M2, as it is used to produce the mounting structures. When assembling the lens into the mount, it is important to consider the expected stresses of the PSE to prevent failure, such as breaking. The Von-Mises stress plots of the PSE are in Figure 7. The maximum allowable bending stress of the printed material is 70 $\mathrm{N/mm^2}$, which is lower in both axial and radial direction.

The force applied to the lens by the force transmitter is 10 N. It represents the maximum radial clamping force of the PSE design, considering the highest expected modulus of elasticity of the printing material and variations in the geometry of the spring elements. As a result, the maximum compressive stress beneath the lens surface is 5 $\mathrm{N/mm^2}$, caused by Hertzian contact pressure. This is well below the typical compressive stress limit of 345 $\mathrm{N/mm^2}$ for optical glass and is therefore not considered critical [25].

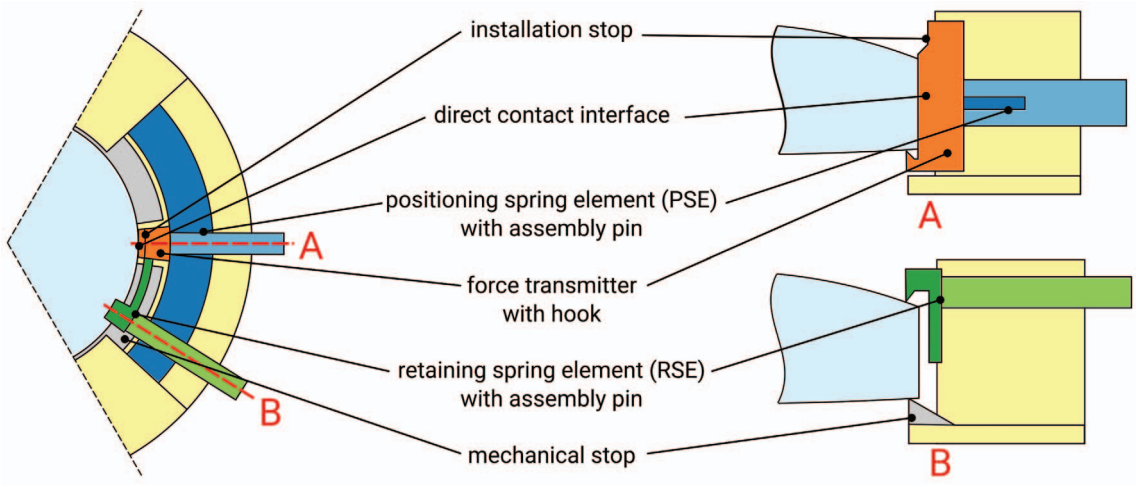

Figure 5. Sketch of an assembled lens in the monolithic mount with printed spring elements. On the left side is the top down view on the mount. Shown is one of the equally spaced mounting units. On the top right the cross-section along the red dashed line marked with A is depicted. It shows the lens in contact with the direct contacting interface, the cross-section of the positioning spring element (PSE) and its assembly pin. The cross-section along the line marked with B is shown on the bottom right. It shows the retaining spring element (RSE) with its assembly pin in contact with the surface of the lens. Also visible is the mechanical stop on which the PSE tensions the lens.

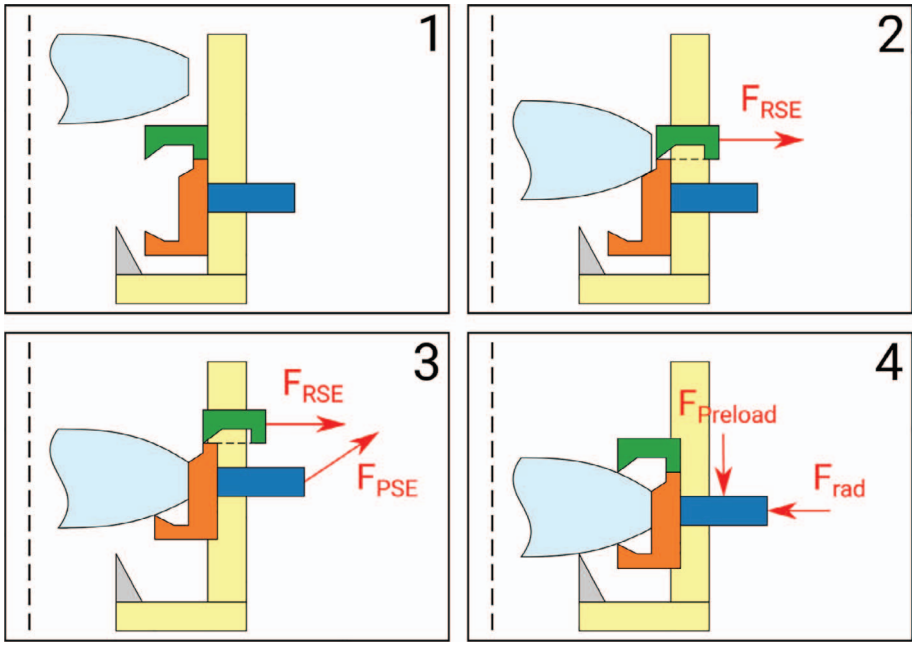

Figure 6. Cross-section view of the assembly process of the lens in the fully monolithic mount. Visible are the PSE (blue), the RSE (green), the lens (light blue), the mechanical stop (grey) and the force transmitter with hook (orange) in the surrounding mounting structure (yellow).

The side view on a demonstrator for this design concept without the RSE is shown in Figure 8. At the top is the mount before the lens is inserted, on the bottom the mount after the lens is inserted. Both depictions are split in half, with the left side representing the simulation and the right side the 3D printed model. It can be observed that the PSE undergoes upward deformation after the lens is mounted, in comparison to its initial state. Additionally, the gap between the force transmitter and the surrounding mounting structure widens. This deformation of the PSE tensions the lens against the mechanical stop and defines its position. The demonstrator was intentionally printed with enlarged deformations to better illustrate the deformation behaviour of the PSE.

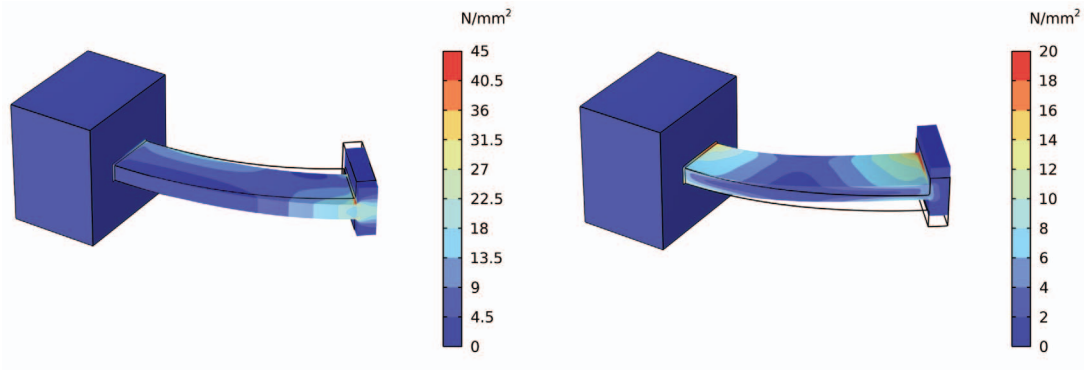

(a) (b)

Figure 7. Plots of the Von-Mises stress from the finite element analysis of the PSE: (a) Von-Mises stress in radial direction; (b) Von-Mises stress in axial direction.

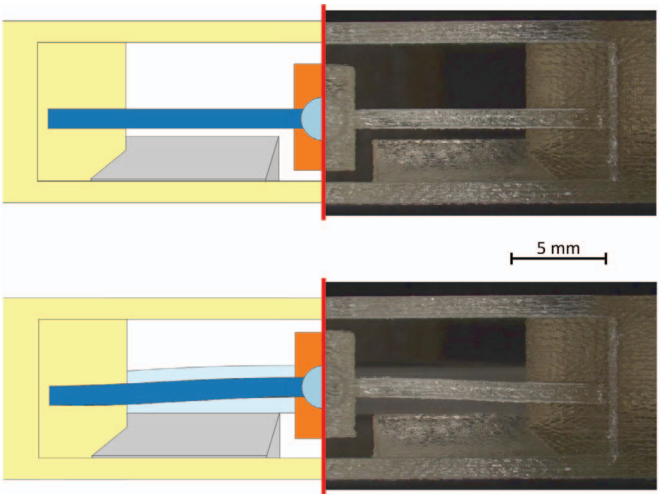

Figure 8. Side view of a lens mounting structure demonstrator without the RSE. The top shows the mount before lens insertion, while the bottom depicts the lens inserted in the mount. Both depictions are split into simulation (left) and 3D printed model (right). After the lens insertion, the PSE (blue) exhibits an upward deformation and an increased gap between the force transmitter (orange) and the surrounding mounting structure (yellow). For illustrative purposes, the demonstrator was deliberately printed with larger deformations than required for the final design.

2.4 Comparison to other flexure mounts

The presented design concept shares similarities with flexure mounts that use the force equilibrium of their spring elements to reposition the optical elements [26]. However, flexure mounts are costly to produce, requiring a lot of components and resulting in a high assembly effort and time. The large number of individual components raises difficulties regarding precise alignment. To compensate, flexure mounting structures for multiple elements are adjustable relative to each other, with accuracy depending on the precision of the adjustment mechanisms. In contrast, our design is enabled by additive manufacturing and requires only one part, simplifying the manufacturing, assembly and alignment process by combining all components into a single monolithic solid body. With conventional manufacturing techniques such mounting structures are not possible to produce.

Moreover, the spring elements in our design concept not only ensure the repositioning of the optical elements, but they can also be adjusted to define a certain initial positioning, compensating manufacturing tolerances of the optical elements. In case of lenses typical tolerances are the so called inner decentration, which describes a lateral offset of the first lens surface vertex to the second surface vertex. This can be compensated by accordingly rolling the lens in its mechanical stop. However, this compensation is a multistep sequential process that requires first to mount the lens, then to measure its positioning or the optical system performance and finally applying the correction with adjustable mechanisms.

Since AM allows to produce individual and very precise structures, mechanical stops defining position of the optical elements can become part of the monolithic mounting structure. This allows to manufacture individual structures in which the mountings for the single lenses are specifically tilted and decentered. These are exactly adjusted to compensate for the inner decentration of the individual lenses that are to be assembled, which can be measured on the unmounted lenses in a preceding step. The range of adjustment is limited by the manufacturing process and not the mounting concept. Thus we only depend on the resolution and accuracy of the 3D printer and not an subsequent assembly or alignment processes of multiple optical and mechanical components.

3 Experimental verification

3.1 Experimental setup and design

The experimental design aims to demonstrate the two key features of our concept. Firstly, we will show that it has a

Table 1. Triplet lens surface data.

Surface No	Radius (mm)	Thickness	Mechanical diameter (mm)	Material
1	34.53	9.00	25.0	N-BAF10
2	−21.98	2.50	25.0	N-SF10
3	−214.63	15.00	25.0	
4	−217.99	4.06	25.0	N-SF10
5	−24.58	2.50	25.0	N-BAF10
6	35.51	17.00	25.0	
7	34.53	9.00	25.0	N-BAF10
8	−21.98	2.40	25.0	N-SF10
9	−217.63	13.37	25.0	

high positioning accuracy and secondly, that it possesses high mechanical robustness. For this we designed and additively manufactured the mounting structure for a triplet lens, according to our concept, and evaluated its optical performance by measuring the wavefront with the Fizeau interferometer VI-direct from Moeller-Wedel Optical. Especially the low order coma aberration is a useful indicator in this regard, as it is zero on axis for a perfectly aligned system. Centration errors in the optical system increase this aberration, which is caused by the misalignment of the lens vertices with the system axis [27]. The coma of the system is measured both before and after applying a mechanical shock of 15G to verify the mechanical stability and ability to reposition the optical elements in the mounting structure.

The triplet consists of three achromatic lenses, the surface data is shown in Table 1. The cross-sections of both the optical design and the 3D model of the monolithic mounting structure, along with the printed and assembled lens, are shown in Figure 9. The complete mounting structure comprises three direct mounting domains and two indirect mounting domains which are realized with a simple solid material connection in between.

We produce the mounting structure with the material jetting 3D-printer Keyence Agilista 3200 using their polyacrylic printing material AR-M2. It has two print heads, one for the model material and one for the support material, which dispenses droplets with a resolution of 40 µm onto its building platform and soldifies them afterwads with an UV-light. Each printing layer has a thickness of 15 µm. The support material is soluble in water and is removed through submersion. After cleaning, the monolithic mounting structures are air-dried at room temperature for three days. Subsequently, the lenses are mounted and then the entire measurement cycle is executed.

The spring elements of the mounting structure are manufactured to attain a positioning accuracy of 6 µm with the design parameters specified in Table 2. The spring parameters are the same for all three lenses, given their nearly identical weights of 20 g and 24 g, respectively. The intention is to minimize the axial preload to barely press the lens against the mechanical stop and minimize the resulting friction forces to achieve a higher positioning accuracy. We established the static friction coefficient μ_s between the printed material and the surfaces of the lenses to be 0.270.01 in an inclinded plane test.

According to the data sheet, the Young's modulus of Keyence AR-M2 ranges from 1870 MPa to 2182 MPa. Nevertheless, this variation has hardly any influence on the achievable position accuracy and causes a difference of less than 0.1 µm. Since the resulting forces of the spring element in both axial and radial directions scale linearly with Young's modulus, only the weight force of the lens is constant. This leads to a slight change in the ratio of the total axial preload, comprising weight force of the lens and the spring forces in the axial direction, to the radial forces.

Typical accelerations during normal handling and usage of optics are assumed to be approximately 3G [26]. Our concept allows for larger accelerations during usage by adjusting the axial preload accordingly. If accelerations surpass the specified limits, like during transport or assembly, temporary displacement of the optical elements occurs, followed by repositioning after this event. An additional advantage of the monolithic design, in comparison to conventional multi-component approaches, is the prevention of irreversible displacements between the components of the optic, further increasing its robustness.

The designed axial preload and therefore the maximum allowable acceleration during usage is 10G. Although this is greater than the desired 3G, it still achieves a positioning accuracy of 6 µm. This results thicker bending springs in the axial direction than necessary, but the disadvantages of a further decrease are not acceptable. Thinner bending springs cause twisting and buckling effects, which compromise the ability to maintain a well-defined axial preload, required for achieving precise element positioning. Moreover, the radial spring stiffness would also be affected negatively by these unwanted twisting and buckling effects, further impacting its functionality. Another approach to circumvent this, are longer spring elements to reduce the axial preload, but they are not feasible due to the restricted available design volume around the lens cylinder to still maintain a compact optical system.

The mechanical shock is applied using a spring system, with the triplet placed in a cage between two vertically

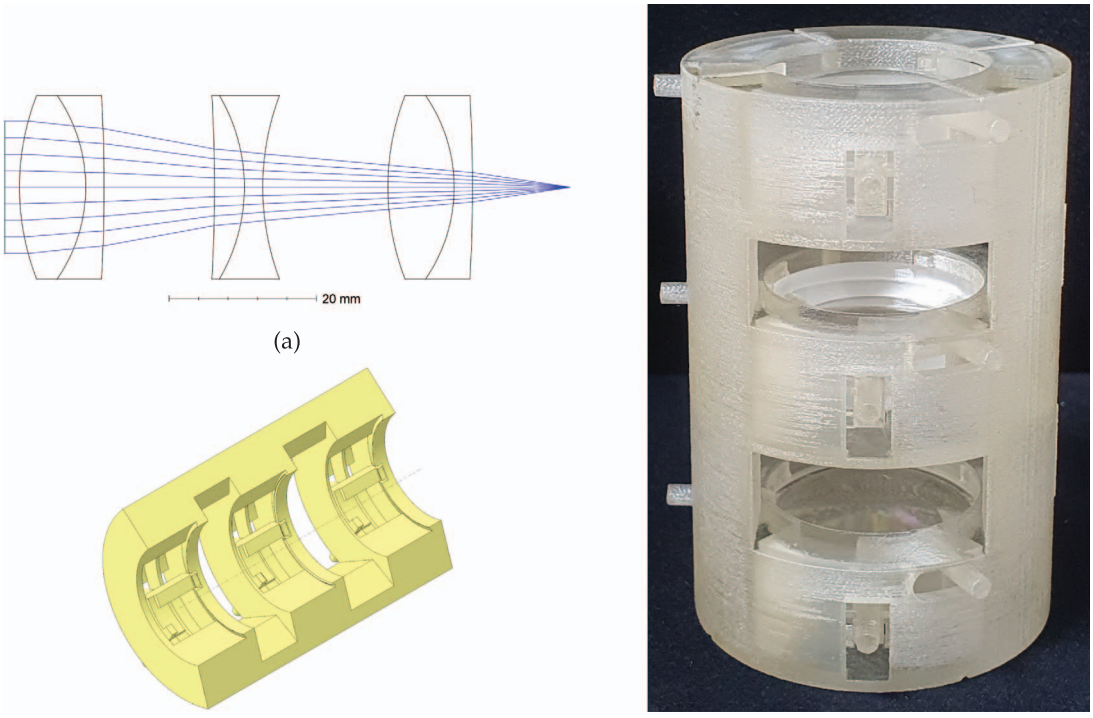

Figure 9. Optical and mechanical design of the triplet: (a) Cross-section of the optical design of the triplet. It consists of three achromatic lenses; (b) Cross-section of the mounting structure. Shown are the three mounts, each with one of their mounting units; (c) Image of the assembled triplet. The lenses are mounted in the 3D-printed mounting structure.

Table 2. Design parameter of the mounting structure. The PSE and RSE in all mounts are the same, because the resulting weight force difference of the lenses is negligible compared to the axial mounting forces and the resulting axial preload. The spring stiffness was calculated with Euler-Bernoulli beam theory. From this design parameters and equation (1) the resulting positioning accuracy could be derived.

Design parameter	Lens 1 and 3	Lens 2
Lens mass in g	24	20
Static friction coefficient μ_s	0.27	0.27
Young's modulus in MPa	1870	1870
PSE parameter		
PSE thickness axial direction in mm	0.9	0.9
PSE thickness radial direction in mm	3.0	3.0
PSE radial spring stiffness in N/mm	57.9	57.9
PSE axial spring stiffness in N/mm	5.2	5.2
RSE parameter		
RSE thickness axial direction in mm	4.0	4.0
RSE thickness radial direction in mm	0.8	0.8
RSE radial spring stiffness in N/mm	2.8	2.8
RSE axial spring stiffness in N/mm	69.8	69.8
Axial preload in N	2.58	2.54
Achievable positioning accuracy in µm	6.0	5.9

arranged springs. The setup and an exemplary acceleration graph is shown in Figure 10. The acceleration is recorded during the experiment with an acceleration sensor and the maximum acceleration, which corresponds to the mechanical shock, is determined. We shocked the triplet once in the axial direction and once in the radial direction with 15G.

3.2 Results and discussion

The wavefront of the triplet was measured with the Fizeau interferometer VI-direct from Moeller-Wedel Optical in double pass. The measurement wavelength is 632 nm. The triplet has an aperture of 18.0 mm and a focal length of 61 mm. From this measurement the coma is derived, which is then correlated with the positioning accuracy of the single lenses in the triplet. The results of the sensitivity analysis by means of simulation as well as the experimental measurement results are depicted in Figure 11.

The simulated coma of the triplet over the so called comparable lens decentration is shown in Figure 11a. For small lens decentrations, the coma exhibits the expected linear behaviour. To evaluate the coma, the comparable lens decentrations of the triplet are simulated. In this system configuration, each lens is radially misaligned by the same amount at an azimuth angular distance of 120°. Furthermore, as a reference, the theoretical achievable positioning accuracy of the designed mounting structure is determined to be 6 µm, by utilizing equation (1) and the design parameters from Table 2. It is important to emphasise that this

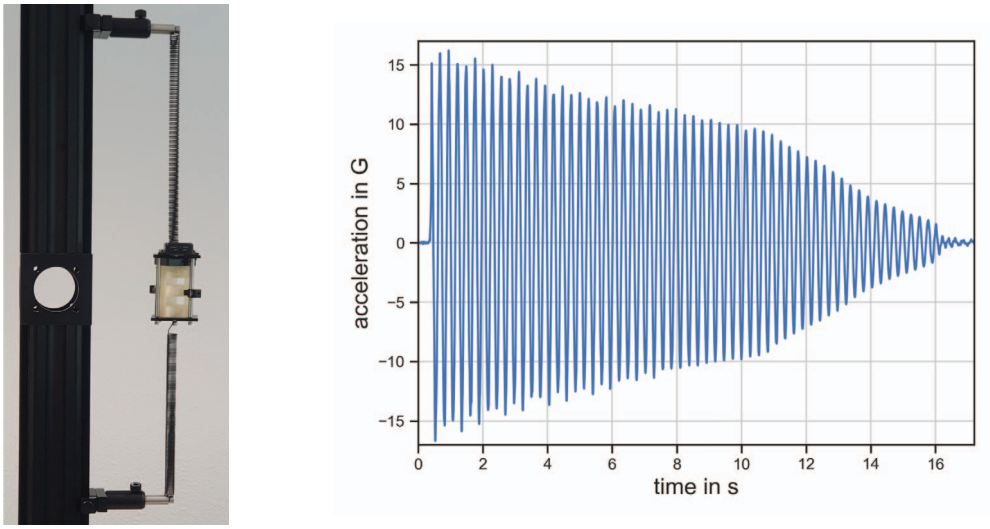

(a) (b)

Figure 10. Acceleration setup to shock the triplet: (a) Image of the shock-test setup. Two springs are vertically arranged with the cage between them, which holds the triplet and acceleration sensor; (b) Exemplary acceleration graph during the shock test.

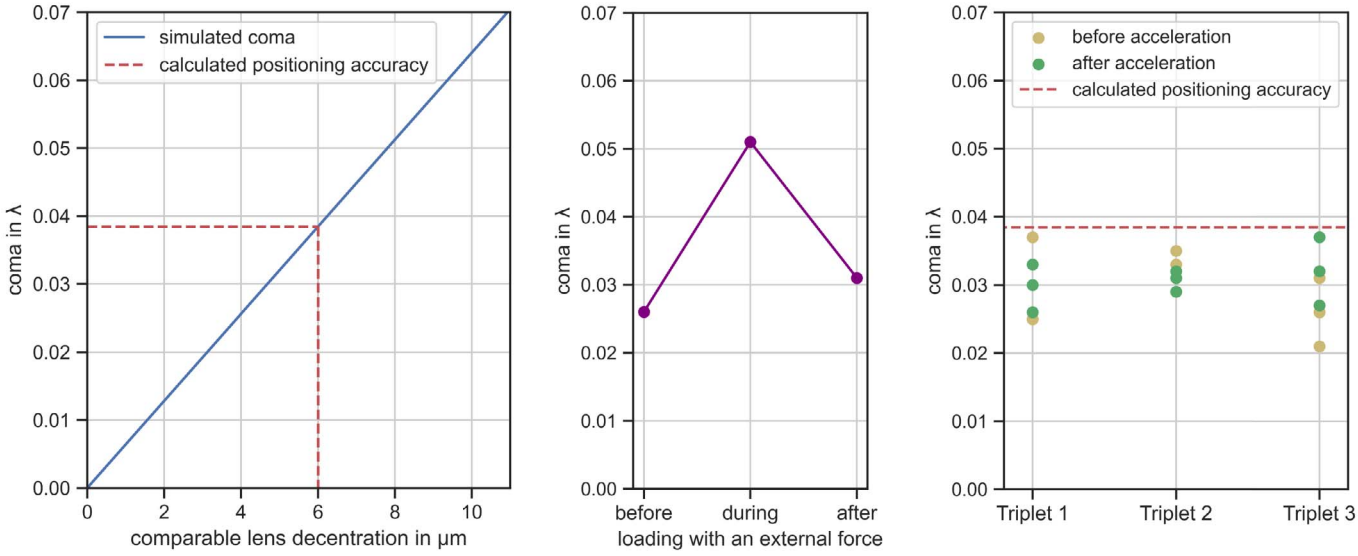

(a) (b) (c)

Figure 11. Simulated sensitivity analysis and results of the measurements: (a) Simulated coma of the triplet over a comparable lens decentration (blue line). The coma is evaluated through simulations of the triplet at comparable lens decentrations, achieved by radially misaligning each lens by the same amount simultaneously at a 120-degree angle from one another. The theoretical achievable positioning accuracy of the designed mounting structure is 6.0 µm, which corresponds to a coma value of 0.038, marked with the red dashed line; (b) Measurements of a mounted triplet before, during, and after the application of a continuous external mechanical force on one PSE from the outside to deliberately displace a single lens in the mount; (c) Experimental results of the triplets before and after applying a 15G mechanical shock to them. The plot also includes the calculated achievable positioning accuracy.

accuracy exceeds the print resolution of 40 µm. This decentration corresponds to a measured coma of 0.038, with being the light wavelength. This is a very small contribution to the overall wavefront error and much smaller than what is typical for optical systems without lens decentration compensation.

To demonstrate that our design actually repositions decentered elements by itself, we applied a continuous external mechanical load on one of the three PSE to deliberately displace the lens. For this, the triplet was measured before, during and after applying the mechanical load. The results are shown in Figure 11b. As can be inferred, the triplet

met the expected specifications both before and after application of the mechanical load, but during the load lens must have been clearly decentered. Due to the external mechanical load, the lens was temporarily pushed farther away from the optical axis, resulting in an increased coma. Upon removal of the load, the remaining imbalance of the radial spring forces is compensated by balancing spring deflections, which push the lenses back towards their respective optimal position. The difference between lens positions before and after applying the mechanical load is within the tolerances due to friction, which is in our case 6 μm.

Finally, the wavefront of three triplets was measured before and after mechanically shocking them with 15G. The results are shown in Figure 11c, along with the coma of the theoretical achievable positioning accuracy. To ensure higher reliability of the measurement, they were repeated it three times, with removing and reinstalling the triplets from the measurement setup. The optical performance of the triplets remained almost the same before and after the mechanical shock. The measurements show that the lenses are positioned with an accuracy better than 6 μm, which is achieved by the resulting balance of forces. In addition, the spring system protects the lenses from 15G accelerations and repositions them afterwards. The springs in axial direction press the lenses against the mechanical stop up to a shock of 10G, after which they deform elastically. Then the lenses temporarily loose contact with the mechanical stop, but are repositioned after the shock event. It is unlikely that all lenses will move uniformly in the same direction and align along another optical axis, so that the coma measurement will be small despite significant misalignment. This can be attributed to the precise repositioning of the single lens after the application of an external mechanical load.

The positioning accuracy, inferred from the wavefront measurements, was better than the predicted 6 μm by the approximation with in equation (1). This can be attributed to several factors. Firstly, the axial forces are slightly lower than their approximation according to the Euler–Bernoulli beam theory, which reduces the resulting friction forces and increases the positioning accuracy. Secondly, measurements of coefficients of friction are inherently dependent on various environmental and operational factors, making them a difficult quantity to measure. This leads to an increase or decrease in the coefficient of static friction, depending on the specific application and environmental conditions. The deviation in the measurement of the static friction coefficient allows a positioning accuracy tolerance of 0.3 μm within our design. Thirdly, the Young's modulus also exhibits variation, scaling both the axial forces and the radial spring stiffness linearly, while the weight force of the lens remains constant. Hence, the resulting friction through the total axial preload varies slightly. This introduces an additional uncertainty of 0.1 μm. Finally, the comparable lens decentration serves as scenario for comparison. Consequently, the observed coma value represents a limit within the acceptable range to which the optical system alignment is still considered to be within specification.

It is noteworthy that the measured values exhibit a comparatively large distribution, which can be attributed to the alignment of the triplet in the measurement setup. Specifically, the optical axis of the triplet is oriented perpendicular to the plane wave of the interferometer, and even slight deviations of 1 arc minute can result in measurable deviations in the positioning accuracy of 0.5 μm, which can be seen here in the distribution of the measured coma values. This means that we do not measure directly on the optical axis, but slightly besides it.

4 Conclusion and outlook

Through the use of additive manufacturing, a monolithic mounting structure has been developed with a mechanical design that allows for precise positioning and mechanical robustness of multiple mounted optical elements. This was achieved with a monolithic mounting structure design, which is a rigid body without any interfaces between the different components of the mechanical system.

An essential feature of the presented concept is the integration of a system of bending spring elements. They generate a well defined force in axial direction to minimize the resulting friction forces, which hinder an accurate positioning of the optical elements in lateral direction, resulting in a remaining decentration. The friction force is overcome with sufficiently large radial spring stiffnesses, which result in large force differences, even for small remaining deflection differences. Although the design of the monolithic mounting structure has similarities with flexure mounts, it differs significantly in that the deformation of the spring elements is used for the initial positioning of the supported elements and for increasing the mechanical robustness of the entire system.

The system of spring elements also absorbs any mechanical shocks, larger than those specified during its usage, and transforms them into elastic deformation, thus increasing the mechanical robustness of the entire optical system. Since these deformations are reversible, the springs return in their original position and push the mounted elements back in their original position. Moreover, the monolithic design further increases its robustness, in preventing irreversible displacements, which are a concern in conventional multi-component designs. The design is adaptable to meet specific mechanical environmental requirements by adjusting the dimensions of the spring elements. However, the trade-off between positioning accuracy and axial preload, which corresponds expected acceleration during its usage, has to be taken into account.

The measurement results demonstrate the design's capability to achieve high positioning accuracy and robustness. It reliably positions the lenses initially and repositions them after severe mechanical influences from the environment, such as shocks. This was evaluated by measuring the wavefront's coma aberration caused by the lens decentrations of a triplet lens, showing that the measurements taken before and after the mechanical shock are almost identical. It was demonstrated that a positioning accuracy better than 6 μm was achieved, which is roughly only 2/10000 of the lens diameter, exceeding the in-plane printer resolution of 40 μm. Consequently, the relative contribution

of these remaining lens decentrations on typical overall wavefront errors is very small. Although lenses were used here for demonstration purposes, the design approach can be used for all different kinds of elements that need to be mounted in any type of optical system.

The proof of principle was established using a mounting structure made from a polyacrylic polymer on a material jetting printer. In this design, the spring elements are permanently under tension stress, which causes creep effects and plastic deformation. Therefore, for future applications, other materials with better long-term durability when exposed to constant mechanical loads are preferable. Possible alternatives include metals like aluminium and steel, as well as other polymers such as PEEK or PAI, known for their high creep resistance.

Based on these results, our design approach will enable the production of precise and mechanically stable mounting structures for optical systems that were previously unattainable, thus laying the foundation for new applications in optics. These structures are particularly useful for optical precision instruments that must to operate in harsh environmental conditions. As a result, our design approach can significantly improve the quality and reliability of optical instruments, enable their application in various fields and facilitate the development of advanced and sophisticated optical devices.

Acknowledgments

We would like to thank Dr. Wolfgang Stolz from the Phillips-University Marburg for his support and feedback.

Funding

This research was realized within the project "Additiv gefertigte Tragstrukturen in optischer Sensorik zur Unterstützung der Technologie-Roadmap des Internet der Dinge" funded by EFRE (European Fond for regional development) and the HMWK (Hessisches Ministerium für Wissenschaft und Kunst).

Conflicts of interest

The authors declare no conflicts of interest.

Data availability statement

Data underlying the results presented in this paper are not publicly available at this time but may be obtained from the authors upon reasonable request.

Author contribution statement

Conceptualization: M.D. and P.P.; methodology: P.P; validation: P.P.; formal analysis: P.P.; investigation: P.P.; resources: M.D.; writing-original draft: P.P.; writing-review and editing: P.P.; visualization: P.P.; supervision: M.D.; funding acquisition: M.D.

References

1 Zolfaghari A, Chen T, Yi AY, Additive manufacturing of precision optics at micro and nanoscale, *Int. J. Extreme Manuf.* **1**, 012005 (2019).

2 Heinrich A, *3D Printing of Optical Components*, **vol. 233**, Springer Series in Optical Sciences (Springer International Publishing, Cham, 2021).

3 Aderneuer T, Fernández O, Ferrini R, Two-photon grayscale lithography for free-form micro-optical arrays, *Opt. Exp.* **29**, 39511–39520 (2021).

4 Toulouse A, Drozella J, Motzfeld P, Fahrbach N, Aslani V, Thiele S, Giessen H, Herkommer AM, Ultra-compact 3D-printed wide-angle cameras realized by multi-aperture free-form optical design, *Opt. Exp.* **30**, 707–720 (2022).

5 Kubec A, Zdora M-C, Sanli UT, Diaz A, Vila-Comamala J, David C, An achromatic X-ray lens, *Nature Commun.* **13**, 1305 (2022).

6 Blachowicz T, Ehrmann G, Ehrmann A, Optical elements from 3D printed polymers, *e-Polymers* **21**, 549–565 (2021).

7 Roulet M, Atkins C, Hugot E, Snell R, Van de Vorst B, Morris K, Marcos M, Todd I, Miller C, Dufils J, Farkas S, Mezo G, Tenegi F, Vega-Moreno A, Schnelter H, Use of 3D printing in astronomical mirror fabrication, in: *3D Printed Optics and Additive Photonic Manufacturing II*, **vol. 11349**: (SPIE, 2020), pp. 33–44.

8 Zhang K, Qu H, Guan H, Zhang J, Zhang X, Xie X, Yan L, Wang C, Design and fabrication technology of metal mirrors based on additive manufacturing: a review, *Appl. Sci.* **11**, 10630 (2021).

9 Chen X, Liu W, Dong B, Lee J, Ware HOT, Zhang HF, Sun C, High-speed 3D printing of millimeter-size customized aspheric imaging lenses with sub 7 nm Surface roughness, *Adv. Mater.* **30**, 1705683 (2018).

10 Delmans M, Haseloff J, Cube: A framework for 3D printable optomechanics, *J. Open Hardware* **2**, 2 (2018).

11 Diederich B, Lachmann R, Carlstedt S, Marsikova B, Wang H, Uwurukundo X, Mosig AS, Heintzmann R, A versatile and customizable low-cost 3D-printed open standard for microscopic imaging, *Nature Commun.* **11**, 5979 (2020).

12 Elías-García A, Hernandez-Martinez CA, Esqueda-Almanza R, Rojas-Santana A, Sánchez-Osorio I, Fast fabrication of optomechanical mounts using additive manufacturing, in: *Optical Design and Fabrication 2021* (Optica Publishing Group, New York, 2021).

13 Nuñez I, Matute T, Herrera R, Keymer J, Marzullo T, Rudge T, Federici F, Low cost and open source multi-fluorescence imaging system for teaching and research in biology and bioengineering, *PLoS ONE* **12**, e0187163 (2017).

14 Yang S, Tang Y, Zhao YF, A new part consolidation method to embrace the design freedom of additive manufacturing, *J. Manufac. Process.* **20**, 444–449 (2015).

15 Alfaify A, Saleh M, Abdullah FM, Al-Ahmari AM, Design for additive manufacturing: a systematic review, *Sustainability* **12**, 7936 (2020).

16 Praveena B, Lokesh L, Buradi A, Santhosh N, Praveena B, Vignesh R, A comprehensive review of emerging additive manufacturing (3D printing technology): Methods, materials, applications, challenges, trends and future potential, *Mater. Today: Proc.* **52**, 1309–1313 (2022).

17 Collins JT, Knapper J, Stirling J, Mduda J, Mkindi C, Mayagaya V, Mwakajinga GA, Nyakyi PT, Sanga VL, Carbery D, White L, Dale S, Lim ZJ, Baumberg JJ, Cicuta P, McDermott S, Vodenicharski B, Bowman R, Robotic microscopy for everyone: The OpenFlexure microscope, *Biomed. Opt. Exp.* **11**, 2447–2460 (2020).

18 Rothermel F, Thiele S, Jung C, Giessen H, Herkommer A, Towards magnetically actuated 3D-printed micro-optical

elements, in *Optomechanics and Optical Alignment*, vol. **11816**:(SPIE, 2021), pp. 134–142.

19 Kranert F, Hinkelmann M, Lachmayer R, Neumann J, Kracht D, Function-integrated laser system based on 3D-printed optomechanics, *Components and packaging for laser systems VIII*, vol. **11982** (SPIE, 2022), pp. 98–104.

20 Erdil K, Gürcüoğlu O, Ferhanoğlu O, Electromagnetically actuated 3D-printed tunable optical slit device, *Appl. Opt.* **62**, 5244–5250 (2023).

21 Li F, Macdonald NP, Guijt RM, Breadmore MC, Increasing the functionalities of 3D printed microchemical devices by single material, multimaterial, and print-pause-print 3D printing, *Lab Chip.* **19**, 35–49 (2019).

22 Espera AH, Dizon JRC, Chen Q, Advincula RC, 3D-printing and advanced manufacturing for electronics, *Prog. Add. Manuf.* **4**, 245–267 (2019).

23 Hai R, Shao G, Ware HOT, Jones EH, Sun C, 3D printing a low-cost miniature accommodating optical microscope, *Adv. Mater.* **35**, 2208365 (2023).

24 Pfuhl P, Degünther M, Compensation of the position errors of optical elements by adapting their additively manufactured mounting structure, in *Opt. Instrum. Sci. Technol. Appl. II*, **Vol. 11876** (SPIE, 2021), pp. 30–36.

25 Schwertz KM, Burge JH, *Field guide to optomechanical design and analysis*, **vol. FG26** (SPIE, Bellingham, WA, USA, 2012)

26 Yoder P, Vukobratovich D, *Opto-mechanical systems design: design and analysis of opto-mechanical assemblies*, **Vol. 1** (Taylor & Francis/CRC Press, Boca Raton, 2015)

27 Fischer RE, Tadic-Galeb B, Yoder PR, *Optical System Design*, 2nd edn. (McGraw-Hill, New York, 2008)